



# First observation of the Cabibbo-suppressed decays $\Xi_c^+ \rightarrow \Sigma^+ \pi^- \pi^+$ and $\Xi_c^+ \rightarrow \Sigma^- \pi^+ \pi^+$ and measurement of their branching ratios

SELEX Collaboration

E. Vázquez-Jáuregui<sup>m</sup>, J. Engelfried<sup>m,\*</sup>, U. Akgun<sup>p</sup>, G. Alkhazov<sup>k</sup>, J. Amaro-Reyes<sup>m</sup>, A.G. Atamantchouk<sup>k,✉</sup>, A.S. Ayan<sup>p</sup>, M.Y. Balatz<sup>h,✉</sup>, A. Blanco-Covarrubias<sup>m</sup>, N.F. Bondar<sup>k</sup>, P.S. Cooper<sup>e</sup>, L.J. Dauwe<sup>q,✉</sup>, G.V. Davidenko<sup>h</sup>, U. Dersch<sup>i,1</sup>, A.G. Dolgolenko<sup>h</sup>, G.B. Dzyubenko<sup>h</sup>, R. Edelstein<sup>c</sup>, L. Emediato<sup>s</sup>, A.M.F. Endler<sup>d</sup>, I. Eschrich<sup>i,2</sup>, C.O. Escobar<sup>s,3</sup>, N. Estrada<sup>m</sup>, A.V. Evdokimov<sup>h</sup>, I.S. Filimonov<sup>j,✉</sup>, F.G. Garcia<sup>s,e</sup>, M. Gaspero<sup>r</sup>, I. Giller<sup>l</sup>, V.L. Golovtsov<sup>k</sup>, P. Gouffon<sup>s</sup>, E. Gülmez<sup>b</sup>, He Kangling<sup>g</sup>, M. Iori<sup>r</sup>, S.Y. Jun<sup>c</sup>, M. Kaya<sup>p,4</sup>, J. Kilmer<sup>e</sup>, V.T. Kim<sup>k</sup>, L.M. Kochenda<sup>k</sup>, I. Konorov<sup>i,5</sup>, A.P. Kozhevnikov<sup>f</sup>, A.G. Krivshich<sup>k</sup>, H. Krüger<sup>i,6</sup>, M.A. Kubantsev<sup>h</sup>, V.P. Kubarovsky<sup>f</sup>, A.I. Kulyavtsev<sup>c,e</sup>, N.P. Kuropatkin<sup>k,e</sup>, V.F. Kurshetsov<sup>f</sup>, A. Kushnirenko<sup>c,f</sup>, S. Kwan<sup>e</sup>, J. Lach<sup>e</sup>, A. Lamberto<sup>t</sup>, L.G. Landsberg<sup>f,✉</sup>, I. Larin<sup>h</sup>, E.M. Leikin<sup>j</sup>, Li Yunshan<sup>g</sup>, G. López-Hinojosa<sup>m</sup>, M. Luksys<sup>n</sup>, T. Lungov<sup>s</sup>, V.P. Maleev<sup>k</sup>, D. Mao<sup>c,7</sup>, Mao Chensheng<sup>g</sup>, Mao Zhenlin<sup>g</sup>, P. Mathew<sup>c,8</sup>, M. Mattson<sup>c</sup>, V. Matveev<sup>h</sup>, E. McCliment<sup>p</sup>, M.A. Moinester<sup>l</sup>, V.V. Molchanov<sup>f</sup>, A. Morelos<sup>m</sup>, K.D. Nelson<sup>p,9</sup>, A.V. Nemitkin<sup>j</sup>, P.V. Neoustroev<sup>k</sup>, C. Newsom<sup>p</sup>, A.P. Nilov<sup>h,✉</sup>, S.B. Nurushev<sup>f</sup>, A. Ocherashvili<sup>l,10</sup>, Y. Onel<sup>p</sup>, E. Ozel<sup>p</sup>, S. Ozkorucuklu<sup>p,11</sup>, A. Penzo<sup>t</sup>, S.V. Petrenko<sup>f</sup>, P. Pogodin<sup>p,12</sup>, M. Procaro<sup>c,13</sup>, V.A. Prutsko<sup>h</sup>, E. Ramberg<sup>e</sup>, G.F. Rappazzo<sup>t</sup>, B.V. Razmyslovich<sup>k,14</sup>, V.I. Rud<sup>j</sup>, J. Russ<sup>c</sup>, J.L. Sánchez-López<sup>m</sup>, P. Schiavon<sup>t</sup>, J. Simon<sup>i,15</sup>, A.I. Sitnikov<sup>h</sup>, D. Skow<sup>e</sup>, V.J. Smith<sup>o</sup>, M. Srivastava<sup>s</sup>, V. Steiner<sup>l</sup>, V. Stepanov<sup>k,14</sup>, L. Stutte<sup>e</sup>, M. Svoiski<sup>k,14</sup>, N.K. Terentyev<sup>k,c</sup>, G.P. Thomas<sup>a</sup>, I. Torres<sup>m</sup>, L.N. Uvarov<sup>k</sup>, A.N. Vasiliev<sup>f</sup>, D.V. Vavilov<sup>f</sup>, V.S. Verebryusov<sup>h</sup>, V.A. Victorov<sup>f</sup>, V.E. Vishnyakov<sup>h</sup>, A.A. Vorobyov<sup>k</sup>, K. Vorwalter<sup>i,16</sup>, J. You<sup>c,e</sup>, Zhao Wenheng<sup>g</sup>, Zheng Shuchen<sup>g</sup>, R. Zukanovich-Funchal<sup>s</sup>

<sup>a</sup> Ball State University, Muncie, IN 47306, USA

<sup>b</sup> Bogazici University, Bebek 80815, Istanbul, Turkey

<sup>c</sup> Carnegie-Mellon University, Pittsburgh, PA 15213, USA

<sup>d</sup> Centro Brasileiro de Pesquisas Físicas, Rio de Janeiro, Brazil

<sup>e</sup> Fermi National Accelerator Laboratory, Batavia, IL 60510, USA

<sup>f</sup> Institute for High Energy Physics, Protvino, Russia

<sup>g</sup> Institute of High Energy Physics, Beijing, PR China

<sup>h</sup> Institute of Theoretical and Experimental Physics, Moscow, Russia

<sup>i</sup> Max-Planck-Institut für Kernphysik, 69117 Heidelberg, Germany

<sup>j</sup> Moscow State University, Moscow, Russia

<sup>k</sup> Petersburg Nuclear Physics Institute, St. Petersburg, Russia

<sup>l</sup> Tel Aviv University, 69978 Ramat Aviv, Israel

<sup>m</sup> Universidad Autónoma de San Luis Potosí, San Luis Potosí, Mexico

<sup>n</sup> Universidade Federal da Paraíba, Paraíba, Brazil

<sup>o</sup> University of Bristol, Bristol BS8 1TL, United Kingdom

<sup>p</sup> University of Iowa, Iowa City, IA 52242, USA

<sup>q</sup> University of Michigan-Flint, Flint, MI 48502, USA

<sup>r</sup> University of Rome "La Sapienza" and INFN, Rome, Italy

<sup>s</sup> University of São Paulo, São Paulo, Brazil

<sup>t</sup> University of Trieste and INFN, Trieste, Italy

## ARTICLE INFO

### Article history:

Received 10 July 2008

Accepted 18 July 2008

Available online 24 July 2008

Editor: W.-D. Schlatter

## ABSTRACT

We report the first observation of two Cabibbo-suppressed decay modes,  $\Xi_c^+ \rightarrow \Sigma^+ \pi^- \pi^+$  and  $\Xi_c^+ \rightarrow \Sigma^- \pi^+ \pi^+$ . We observe  $59 \pm 14$  over a background of 87, and  $22 \pm 8$  over a background of 13 events, respectively, for the signals. The data were accumulated using the SELEX spectrometer during the 1996–1997 fixed target run at Fermilab, chiefly from a 600 GeV/c  $\Sigma^-$  beam. The branching ratios of the decays

PACS:  
13.30.-a  
13.30.Eg  
14.20.Lq

relative to the Cabibbo-favored  $\Xi_c^+ \rightarrow \Xi^- \pi^+ \pi^+$  are measured to be  $B(\Xi_c^+ \rightarrow \Sigma^+ \pi^- \pi^+)/B(\Xi_c^+ \rightarrow \Xi^- \pi^+ \pi^+) = 0.48 \pm 0.20$ , and  $B(\Xi_c^+ \rightarrow \Sigma^- \pi^+ \pi^+)/B(\Xi_c^+ \rightarrow \Xi^- \pi^+ \pi^+) = 0.18 \pm 0.09$ , respectively. We also report branching ratios for the same decay modes of the  $\Lambda_c^+$  relative to  $\Lambda_c^+ \rightarrow pK^- \pi^+$ .

© 2008 Elsevier B.V. All rights reserved.

## 1. Introduction

Studying Cabibbo-suppressed (CS) decays of hadrons provides insights into the weak interaction mechanism for non-leptonic decays [1]. Comparing the strengths of CS decays to their Cabibbo-favored (CF) analogs, one can, in a systematic way, assess the contributions of the various mechanisms. In addition, comparing the same or similar decay modes of different baryons allows some additional insights. Even though any CS decay mode of the  $\Xi_c^+$  is a CF mode of the  $\Lambda_c^+$ , the detailed arrangement of the different final-state quarks into hadrons might be different, as shown in the spectator diagrams in Figs. 1 and 2. While in the case of the  $\Lambda_c^+$  both final-state baryons, the  $\Sigma^+$  and the  $\Sigma^-$ , can have the  $s$  quark resulting from the CF  $c$  decay, in the case of the  $\Xi_c^+$  decays with the identical final-state hadrons, only the  $\Sigma^-$  can be formed with the CS  $c$  decay product. By comparing several decay modes of different hadrons some information about the importances of direct quark emission at the decay stage and from quark rearrangement due to final-state scattering might be obtained.

Modern methods for calculating non-leptonic decay rates of the charm hadrons employ heavy quark effective theory and the factorization approximation [2]. Nonetheless, the three-body decays of charm baryons are prohibitively difficult to calculate due to the complexity of associated final-state interactions. Measurements of the relative branching fractions of charm baryon states, both CF and CS, give additional information about the structure of the decay amplitude and the validity of the factorization approximation.

Until now, the only CS  $\Xi_c^+$  decays reported are  $\Xi_c^+ \rightarrow pK^- \pi^+$  [3,4] and  $\Xi_c^+ \rightarrow \Sigma^+ K^- K^+$  [5]. In this Letter, we present the first observations of  $\Xi_c^+ \rightarrow \Sigma^+ \pi^- \pi^+$  and  $\Xi_c^+ \rightarrow \Sigma^- \pi^+ \pi^+$ , and determine their branching ratios relative to the CF  $\Xi_c^+ \rightarrow \Xi^- \pi^+ \pi^+$ . To validate our analysis method, we also report the branching ratios  $B(\Lambda_c^+ \rightarrow \Sigma^+ \pi^- \pi^+)/B(\Lambda_c^+ \rightarrow pK^- \pi^+)$  and  $B(\Lambda_c^+ \rightarrow \Sigma^- \pi^+ \pi^+)/B(\Lambda_c^+ \rightarrow \Sigma^+ \pi^- \pi^+)$  and compare them to previously reported results [6–8].

\* Corresponding author.

E-mail address: jurgen@fisica.uaslp.mx (J. Engelfried).

<sup>1</sup> Present address: Advanced Mask Technology Center, Dresden, Germany.

<sup>2</sup> Present address: University of California at Irvine, Irvine, CA 92697, USA.

<sup>3</sup> Present address: Instituto de Física da Universidade Estadual de Campinas, UNICAMP, SP, Brazil.

<sup>4</sup> Present address: Kafkas University, Kars, Turkey.

<sup>5</sup> Present address: Physik-Department, Technische Universität München, 85748 Garching, Germany.

<sup>6</sup> Present address: The Boston Consulting Group, München, Germany.

<sup>7</sup> Present address: Lucent Technologies, Naperville, IL, USA.

<sup>8</sup> Present address: Baxter Healthcare, Round Lake, IL, USA.

<sup>9</sup> Present address: University of Alabama at Birmingham, Birmingham, AL 35294, USA.

<sup>10</sup> Present address: NRCN, 84190 Beer-Sheva, Israel.

<sup>11</sup> Present address: Süleyman Demirel Üniversitesi, Isparta, Turkey.

<sup>12</sup> Present address: Legal Department, Oracle Corporation, Redwood Shores, California, USA.

<sup>13</sup> Present address: DOE, Germantown, MD, USA.

<sup>14</sup> Present address: Solidum, Ottawa, Ontario, Canada.

<sup>15</sup> Present address: Siemens Healthcare, Erlangen, Germany.

<sup>16</sup> Present address: Allianz Insurance Group IT, München, Germany.

✘ Deceased.

## 2. Experiment

SELEX is a high energy hadroproduction experiment using a 3-stage spectrometer designed for high acceptance for forward ( $\chi_F \gtrsim 0.1$ ) interactions. The main goal of the experiment is the study of production and decay properties of charm baryons. Particles in the negative (600 GeV/c,  $\simeq 50\% \Sigma^-$ ,  $\simeq 50\% \pi^-$ ) and positive beam (540 GeV/c,  $\simeq 92\% p$ ,  $\simeq 8\% \pi^+$ ) were tagged by a beam transition radiation detector. The data were accumulated from a five-foil segmented target (2 Cu, 3 C, each separated by 1.5 cm) with a total thickness of 5% of an interaction length for protons. The spectrometer had silicon strip detectors to measure the beam and outgoing tracks, giving precision primary and secondary vertex reconstruction. Momenta of particles deflected by the analyzing magnets were measured by a system of proportional wire chambers (PWCs), drift chambers and silicon strip detectors. Momentum resolution for a typical 100 GeV/c track was  $\sigma_p/p \approx 0.5\%$ . Charged particle identification was performed with a Ring Imaging Cherenkov detector (RICH) [9], which distinguished  $K^\pm$  from  $\pi^\pm$  up to 165 GeV/c. The proton identification efficiency was  $>95\%$  above proton threshold ( $\approx 90$  GeV/c). For pions reaching the RICH detector, the total mis-identification probability due to all sources of confusion was  $<4\%$ .

Interactions were selected by a scintillator trigger. The trigger for charm required at least 4 charged tracks after the targets as indicated by an interaction counter and at least 2 hits in a scintillator hodoscope after the second analyzing magnet. It accepted about 1/3 of all inelastic interactions. Triggered events were further tested in an on-line computational filter based on downstream tracking and particle identification information. The on-line filter selected events that had evidence of a secondary vertex from tracks completely reconstructed using the forward PWC spectrometer and the vertex silicon. This filter reduced the data size by a factor of nearly 8 at a cost of about a factor of 2 in charm yield. From a total of  $15.2 \times 10^9$  interactions during the 1996–1997 fixed target run about  $10^9$  events were written to tape. A more detailed description of the apparatus can be found elsewhere [3,10].

## 3. Data analysis

In this analysis, secondary vertex reconstruction was attempted when the  $\chi^2$  per degree of freedom for the fit of the ensemble of charged tracks to a single primary vertex exceeded 4. All combinations of tracks were formed for secondary vertices (in a first step with  $\chi_{\text{sec}}^2 < 9$ , but harder cut values were applied at later stages) and tested against a reconstruction table that specified selection criteria for each charm decay mode. Secondary vertices which occurred inside the volume of a target were rejected. Common identification criteria for the different decay modes were: proton and kaon candidate tracks were required to be identified by the RICH detector to be at least as likely as a pion; if a pion candidate track reached the RICH detector, we applied as a loose requirement that it had to have a likelihood of at least 10%, otherwise it was always accepted; hyperon ( $\Sigma^\pm$ ,  $\Xi^-$ ) decays were identified by disappearance of a track in a limited decay interval (5–12 m downstream from the target), requiring that the candidate track had hits in the tracking detectors before the first and in-between the first and second magnet, but no hits assigned along the extrapolated trajectory

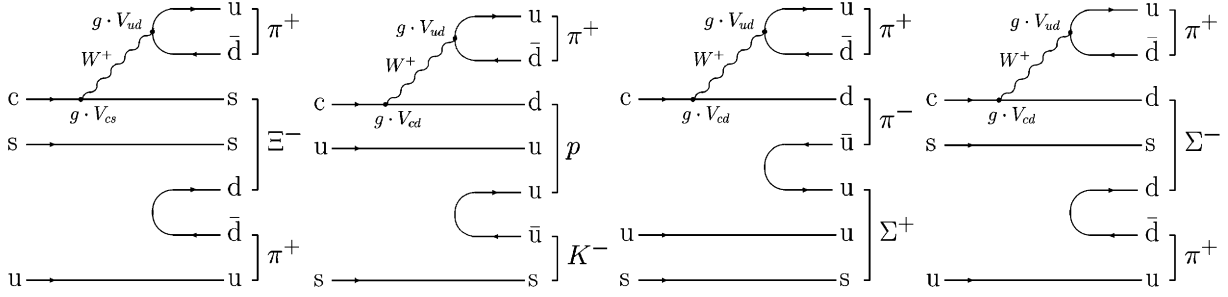


**Fig. 1.** Spectator diagrams for the decays (from left to right)  $\Xi_c^+ \rightarrow \Xi^- \pi^+ \pi^+$ ,  $\Xi_c^+ \rightarrow p K^- \pi^+$ ,  $\Xi_c^+ \rightarrow \Sigma^+ \pi^- \pi^+$ , and  $\Xi_c^+ \rightarrow \Sigma^- \pi^+ \pi^+$ . The corresponding  $W$ -exchange diagrams and additional final-state quark rearrangements are not shown here.

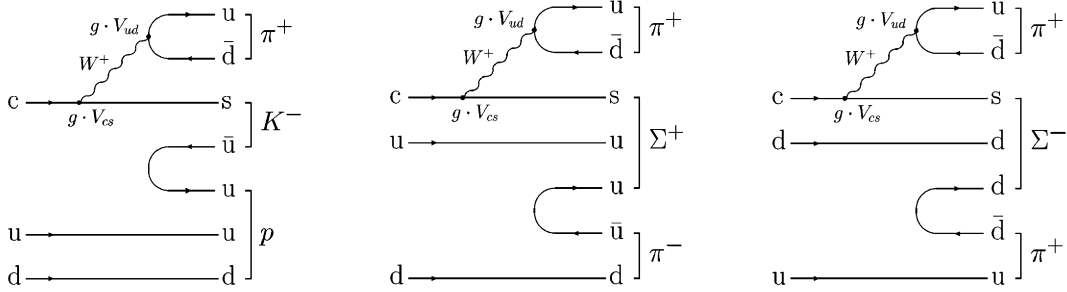


**Fig. 2.** Spectator diagrams for the decays  $\Lambda_c^+ \rightarrow p K^- \pi^+$  (left),  $\Lambda_c^+ \rightarrow \Sigma^+ \pi^- \pi^+$  (middle), and  $\Lambda_c^+ \rightarrow \Sigma^- \pi^+ \pi^+$  (right). The corresponding  $W$ -exchange diagrams and additional final-state quark rearrangements are not shown here.

in the 14 chambers after the second analyzing magnet; this category of tracks gives unique  $\Sigma^+$  identification but is ambiguous between  $\Sigma^-$  and  $\Xi^-$ . Additional ambiguities in the mass assignments may arise due to loose particle identification criteria for  $p$ ,  $K^\pm$ , and  $\pi^\pm$ ; tighter cuts on the identification criteria would reduce the accessible momentum range and the number of observed events.

As additional cuts with variable values depending on the decay modes and the relative branching ratio to be determined we used:

- the separation between the primary and secondary vertices in units of its error ( $L/\sigma$ ) and the error itself ( $\sigma$ );
- the reconstructed charm momentum vector point-back to the primary vertex, expressed as the square of the distance of the reconstructed charm momentum vector to the primary vertex in the target plane in units of its error ( $p_{vtx}$ );
- the sum of the squares of the transverse momenta of the daughter tracks with respect to the charm hadron direction of flight ( $\Sigma_{pt^2}$ );
- the second-largest miss-distance of the daughter tracks in the target plane in units of its error ( $scut$ );
- minimum momenta for the  $\pi^\pm$  ( $p_\pi$ ) and hyperon ( $p_{hyp}$ ) daughter tracks.

The selection criteria and the actual values for these cuts are discussed in the following sections and are listed in Tables 2 and 3.

The total acceptance (geometrical acceptance and reconstruction efficiencies) for the different decay modes of interest was estimated by embedding Monte Carlo charm decay tracks into data events. Momentum and energy were not conserved in the process, but studies indicate this has little effect on the single-charm acceptance calculation. Events were generated with an average transverse momentum ( $p_T$ ) = 1.0 GeV/c and longitudinal momentum distributions according to  $(1 - x_F)^n$ , with  $n = 2.5$  ( $n = 2.45 \pm 0.18$  for  $\Lambda_c^+$  production with a  $\Sigma^-$  beam [11]). The value of  $n$  was varied during the systematic studies and did not affect the final branching ratio results. Detector hits, including resolution and multiple Coulomb scattering smearing effects, produced by these

**Table 1**

Results of the Gaussian parts of the fits to the distributions presented in Fig. 3

Mode	Mass [MeV/c <sup>2</sup> ]	Events	Mass [MeV/c <sup>2</sup> ]	Events
$\Sigma^+ \pi^- \pi^+$	$2288.1 \pm 2.2$	$74.2 \pm 13.8$	$2471.6 \pm 3.9$	$58.7 \pm 13.5$
$\Sigma^- \pi^+ \pi^+$	$2286.0 \pm 1.8$	$46.4 \pm 10.1$	$2463.3 \pm 3.0$	$22.3 \pm 7.5$

embedded tracks were folded into the hit banks of the underlying data event. The new ensemble of hits was passed through the SELEX off-line software. The acceptance is the ratio of the number of reconstructed events to the number of embedded events in a particular mode. For the determination of the branching ratios only the relative acceptances are relevant, leading to a cancellation of most systematic effects associated with the acceptance corrections.

#### 4. First observation of $\Xi_c^+ \rightarrow \Sigma^+ \pi^- \pi^+$ and $\Xi_c^+ \rightarrow \Sigma^- \pi^+ \pi^+$

In Fig. 3 we show the invariant mass distributions of  $\Sigma^+ \pi^- \pi^+$  and  $\Sigma^- \pi^+ \pi^+$ , over the full mass range evaluated. In each distribution we can see two peaks, corresponding to the  $\Lambda_c^+$  and  $\Xi_c^+$  decays. The cuts used for the two distributions are shown in the first two rows of Tables 2 and 3. Additionally we required in both channels that at least one of the pions reached the RICH detector. For  $\Sigma^+ \pi^- \pi^+$  we applied  $\sigma < 0.10$  cm,  $\chi_{sec}^2 < 7$ ,  $p_{hyp} > 70$  GeV/c and events with an invariant mass around the  $\Xi_c^+$  mass in the  $\Sigma^+ K^- \pi^+$  interpretation were removed; for  $\Sigma^- \pi^+ \pi^+$   $\sigma < 0.08$  cm,  $\chi_{sec}^2 < 6$ ,  $p_{hyp} > 80$  GeV/c,  $scut > 4$  and events with an invariant mass around the  $\Xi_c^+$  mass in the  $\Xi_c^+ \pi^+ \pi^+$  interpretation were removed. The selection of the individual cut values was based on prior SELEX analyzes and tuned to suppress backgrounds mostly present in the  $\Xi_c^+$  mass region. To both distributions we adjust the sum of two Gaussians with fixed widths (given by Monte Carlo) and a second degree polynomial. The results of the fits are summarized in Table 1. For the decay  $\Xi_c^+ \rightarrow \Sigma^+ \pi^- \pi^+$  we observe  $S = 58.7 \pm 13.5$  signal events over a background of  $B = 87.3 \pm 6.7$ , corresponding to a significance  $S/\sqrt{B} = 6.3 \pm 1.5$ . For the decay  $\Xi_c^+ \rightarrow \Sigma^- \pi^+ \pi^+$  we observe  $S = 22.3 \pm 7.5$  sig-

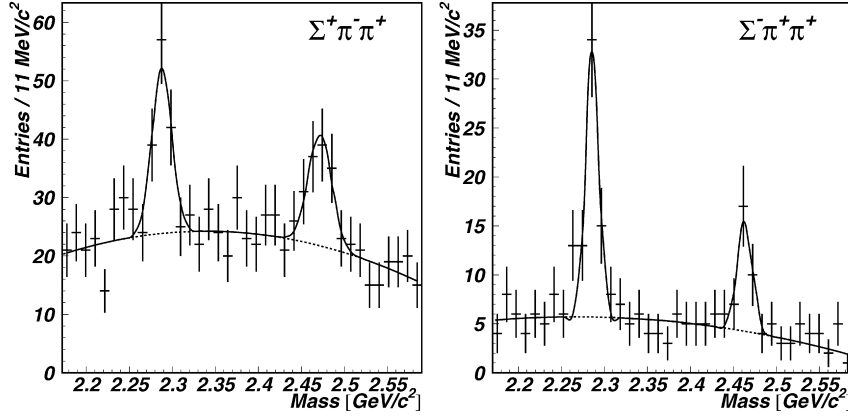


Fig. 3. Invariant mass distributions of  $\Sigma^+\pi^-\pi^+$  (left) and  $\Sigma^-\pi^+\pi^+$  (right).

nal events over a background of  $B = 12.8 \pm 2.5$ , corresponding to a significance  $S/\sqrt{B} = 6.2 \pm 2.2$ . The masses of both the  $\Lambda_c^+$  and the  $\Xi_c^+$  are slightly higher (in the case of  $\Sigma^+\pi^-\pi^+$ ) and lower ( $\Sigma^-\pi^+\pi^+$ ) than the nominal values. Varying the bin width and the fixed widths of the Gaussians also gives consistent results. We verified that the number of observed events varies as a function of the cut variables, especially  $L$  and  $L/\sigma$ , in the same way as expected from Monte Carlo (e.g. the observed events have the lifetime of the  $\Xi_c^+$ ).

## 5. Measurement of branching ratios

For the different branching ratio measurements we used different selection cuts, chosen under the criteria to minimize systematic effects on the final result. We selected central cut values within a region where the Monte Carlo described well the distributions of all the observables, for both the decay mode of interest and the normalization mode. If the same mode was used in different branching ratio determinations, this selection could result in a different set of cuts. We only used interactions initiated by a  $\Sigma^-$  as beam particle and all decay products (with the exception of the hyperons) had to be within the RICH acceptance and correspondingly identified. In the different modes we removed events stemming from the following reflections due to ambiguities in the mass assignments:  $D^+ \rightarrow K^-\pi^+\pi^+$  (1),  $D^+ \rightarrow K^+K^-\pi^+$  (2),  $D^+ \rightarrow K^+\pi^-\pi^+$  (3),  $D_s^+ \rightarrow K^+K^-\pi^+$  (4),  $D_s^+ \rightarrow K^+\pi^-\pi^+$  (5),  $\Lambda_c^+ \rightarrow p\pi^-\pi^+$  (6),  $\Lambda_c^+ \rightarrow \Sigma^-\pi^+\pi^+$  (7),  $\Lambda_c^+ \rightarrow pK^-\pi^+$  (8),  $\Xi_c^+ \rightarrow \Xi^-\pi^+\pi^+$  (9),  $\Xi_c^+ \rightarrow \Sigma^+K^-\pi^+$  (10). We indicate the removed reflections and the corrections due to the removal in Tables 2 and 3.

In Fig. 4 we show the invariant mass distributions of  $\Sigma^+\pi^-\pi^+$ ,  $\Sigma^-\pi^+\pi^+$ ,  $pK^-\pi^+$ , and  $\Xi^-\pi^+\pi^+$  in the  $\Xi_c^+$  mass region.

To verify our analysis method we determine the relative branching ratios of two  $\Lambda_c^+$  decay modes which are identical to our newly observed  $\Xi_c^+$  modes, using the fact that every CF  $\Lambda_c^+$  decay mode is also a CS  $\Xi_c^+$  mode. In Fig. 5 we show the invariant mass distributions of  $\Sigma^+\pi^-\pi^+$ ,  $\Sigma^-\pi^+\pi^+$ , and  $pK^-\pi^+$  in the  $\Lambda_c^+$  mass region.

The number of observed events was determined by adjusting a Gaussian of fixed width (given by Monte Carlo) and a first-order polynomial to the distributions shown in Figs. 4 and 5.<sup>17</sup> While most of the reflections lie outside of the mass peaks and are removed to smoothen the backgrounds, some of them extend below the peaks and remove good events; we studied this effect carefully

Table 2

Number of observed events and total acceptances for the different  $\Xi_c^+$  decay modes, with the corresponding cuts applied to each mode. Common cuts are:  $\chi_{\text{sec}}^2 < 8$ ,  $\sigma < 0.10$  cm,  $scut > 8$ ,  $p_{\text{hyp}} > 40$  GeV/c. The first two rows refer to the signals shown in Fig. 3, with different common cuts as described in Section 4. “Corrected Events” are the number of observed events plus the corrections due to the removal of reflections and are shown separately in parenthesis; we keep the relative error from the fits

$\Xi_c^+$ mode	$L/\sigma$	$pvtx$	$\Sigma_{pt^2}$ [GeV <sup>2</sup> /c <sup>2</sup> ]	Removed reflections	Corrected events	Acceptance [%]
$\Sigma^+\pi^-\pi^+$	>12	<13	>0.4	(10)	$58.7 \pm 13.5$	0.750
$\Sigma^-\pi^+\pi^+$	>8	<10	>0.5	(9)	$22.3 \pm 7.5$	0.950
$pK^-\pi^+$	>11	<13	>0.3	(1, 2, 4, 6)	$(47.4 + 14.0) \pm 14.0$	4.164
$\Xi^-\pi^+\pi^+$				(7)	$(67.0 + 2.4) \pm 10.9$	0.915
$\Sigma^+\pi^-\pi^+$	>13	<13	>0.35	(6)	$(20.7 + 1.6) \pm 8.6$	0.586
$\Xi^-\pi^+\pi^+$				(7)	$(63.3 + 2.0) \pm 10.4$	0.825
$\Sigma^-\pi^+\pi^+$	>13	<10	>0.35	(2, 3, 5, 9)	$(9.5 + 5.0) \pm 6.4$	0.988
$\Xi^-\pi^+\pi^+$				(7)	$(61.1 + 2.6) \pm 9.3$	0.800
$\Sigma^-\pi^+\pi^+$	>13	<10	>0.35	(2, 3, 5, 9)	$(9.5 + 5.0) \pm 6.4$	0.988
$\Sigma^+\pi^-\pi^+$				(6)	$(18.4 + 1.5) \pm 7.5$	0.570

Table 3

Number of observed events and total acceptances for the different  $\Lambda_c^+$  decay modes, with the corresponding cuts applied to each mode. Common cuts are:  $\chi_{\text{sec}}^2 < 4$ ,  $\sigma < 0.10$  cm,  $scut > 8$ ,  $p_{\text{hyp}} > 40$  GeV/c. The first two rows refer to the signals shown in Fig. 3, with different common cuts as described in Section 4. “Corrected Events” are the number of observed events plus the corrections due to the removal of reflections and are shown separately in parenthesis; we keep the relative error from the fits

$\Lambda_c^+$ mode	$L/\sigma$	$pvtx$	$\Sigma_{pt^2}$ [GeV <sup>2</sup> /c <sup>2</sup> ]	Removed reflections	Corrected events	Acceptance [%]
$\Sigma^+\pi^-\pi^+$	>12	<13	>0.4	(10)	$74.2 \pm 13.8$	0.450
$\Sigma^-\pi^+\pi^+$	>8	<10	>0.5	(9)	$46.4 \pm 10.1$	0.500
$\Sigma^+\pi^-\pi^+$	>11	<7	>0.3	(8)	$(46.6 + 3.0) \pm 9.6$	0.292
$pK^-\pi^+$				-	$(561.2 + 0.0) \pm 25.5$	2.367
$\Sigma^-\pi^+\pi^+$	>11	<4	>0.4	(5, 9)	$(29.7 + 2.2) \pm 6.6$	0.434
$pK^-\pi^+$				-	$(450.7 + 0.0) \pm 22.3$	1.923
$\Sigma^-\pi^+\pi^+$	>11	<4	>0.4	(5, 9)	$(29.7 + 2.2) \pm 6.6$	0.434
$\Sigma^+\pi^-\pi^+$				(8)	$(43.0 + 3.4) \pm 8.1$	0.241

with Monte Carlo and corrected the number of observed events for these losses. To determine the correction we simulated the shape of the invariant mass distribution of the reflected mode (including all cuts) and scaled the number of events below the peak region to the number of observed events in the reflected mode, keeping the same relative error for the number of observed events. We also studied correlations for the cases where more than one reflection was removed and found them to be small and negligible. The corrected yields for the different modes are, along with the

<sup>17</sup> Counting the number of entries above the extrapolated background, and using a second-order polynomial for the background, we obtain within errors the same number of events.

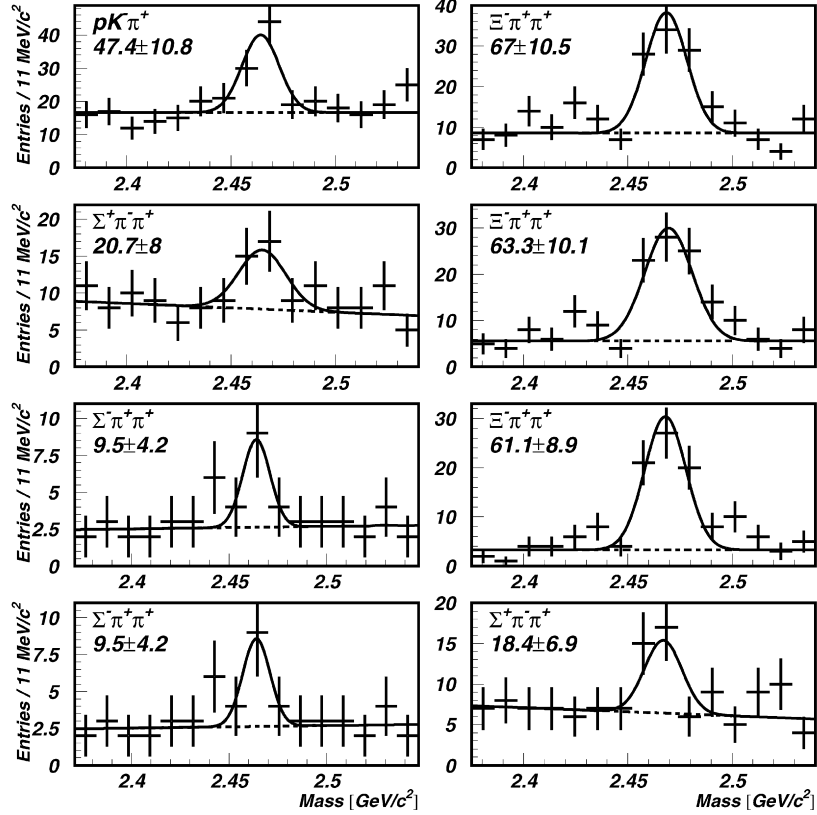


**Fig. 4.** Eight invariant mass distributions of:  $pK^- \pi^+$ ,  $\Sigma^+ \pi^- \pi^+$ ,  $\Sigma^- \pi^+ \pi^+$ ,  $\Xi^- \pi^+ \pi^+$ , used to determine the four relative branching ratios (in pairs from top to bottom)  $B(\Xi_c^+ \rightarrow pK^- \pi^+)/B(\Xi_c^+ \rightarrow \Xi^- \pi^+ \pi^+)$ ,  $B(\Xi_c^+ \rightarrow \Sigma^+ \pi^- \pi^+)/B(\Xi_c^+ \rightarrow \Xi^- \pi^+ \pi^+)$ ,  $B(\Xi_c^+ \rightarrow \Sigma^- \pi^+ \pi^+)/B(\Xi_c^+ \rightarrow \Xi^- \pi^+ \pi^+)$ , and  $B(\Xi_c^+ \rightarrow \Sigma^- \pi^+ \pi^+)/B(\Xi_c^+ \rightarrow \Sigma^+ \pi^- \pi^+)$ , respectively. Different selection cuts were used for each branching ratio (see text). We adjust a Gaussian (fixed width given by Monte Carlo) over a linear background to each of the distributions. The event yields are summarized in Table 2.

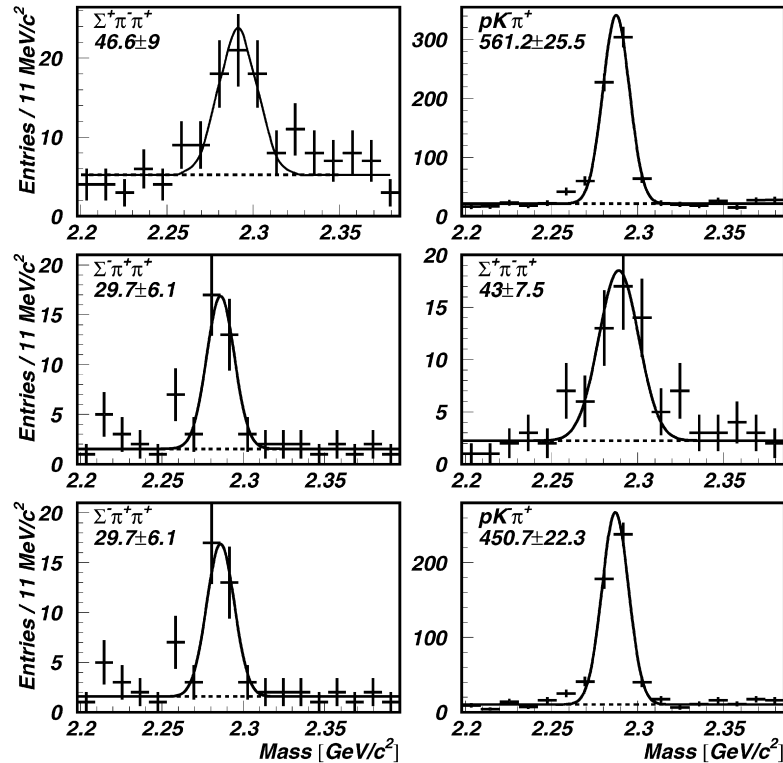


**Fig. 5.** Six invariant mass distributions of:  $\Sigma^+ \pi^- \pi^+$ ,  $pK^- \pi^+$ ,  $\Sigma^- \pi^+ \pi^+$ , used to determine the three relative branching ratios (in pairs from top to bottom)  $B(\Lambda_c^+ \rightarrow \Sigma^+ \pi^- \pi^+)/B(\Lambda_c^+ \rightarrow pK^- \pi^+)$ ,  $B(\Lambda_c^+ \rightarrow \Sigma^- \pi^+ \pi^+)/B(\Lambda_c^+ \rightarrow \Sigma^+ \pi^- \pi^+)$ , and  $B(\Lambda_c^+ \rightarrow \Sigma^- \pi^+ \pi^+)/B(\Lambda_c^+ \rightarrow pK^- \pi^+)$ , respectively. Different selection cuts were used for each branching ratio (see text). We adjust a Gaussian (fixed width given by Monte Carlo) over a linear background to each of the distributions. The event yields are summarized in Table 3.

**Table 4**  
Results of the different branching ratios measured in this analysis, and comparison to previously published results (if available). Also shown is the  $\alpha$ -parameter (see text) for each branching ratio result

Branching ratio	This analysis	Other measurements
$B(\Xi_c^+ \rightarrow \Sigma^+ \pi^- \pi^+)/B(\Xi_c^+ \rightarrow \Xi^- \pi^+ \pi^+)$	$0.48 \pm 0.20$ $\alpha = 6.4 \pm 2.7$	–
$B(\Xi_c^+ \rightarrow \Sigma^- \pi^+ \pi^+)/B(\Xi_c^+ \rightarrow \Xi^- \pi^+ \pi^+)$	$0.18 \pm 0.09$ $\alpha = 2.5 \pm 1.2$	–
$B(\Xi_c^+ \rightarrow \Sigma^- \pi^+ \pi^+)/B(\Xi_c^+ \rightarrow \Sigma^+ \pi^- \pi^+)$	$0.42 \pm 0.24$ $\alpha = 0.43 \pm 0.25$	–
$B(\Xi_c^+ \rightarrow p K^- \pi^+)/B(\Xi_c^+ \rightarrow \Xi^- \pi^+ \pi^+)$	$0.194 \pm 0.054$ $\alpha = 2.6 \pm 0.7$	$0.234 \pm 0.047 \pm 0.022$ [4] $0.20 \pm 0.04 \pm 0.02$ [3]
$B(\Lambda_c^+ \rightarrow \Sigma^- \pi^+ \pi^+)/B(\Lambda_c^+ \rightarrow p K^- \pi^+)$	$0.314 \pm 0.067$ $\alpha = 0.30 \pm 0.07$	–
$B(\Lambda_c^+ \rightarrow \Sigma^+ \pi^- \pi^+)/B(\Lambda_c^+ \rightarrow p K^- \pi^+)$	$0.72 \pm 0.14$ $\alpha = 0.68 \pm 0.14$	$0.74 \pm 0.07 \pm 0.09$ [7] $0.54_{-0.15}^{+0.18}$ [6]
$B(\Lambda_c^+ \rightarrow \Sigma^- \pi^+ \pi^+)/B(\Lambda_c^+ \rightarrow \Sigma^+ \pi^- \pi^+)$	$0.38 \pm 0.10$ $\alpha = 0.39 \pm 0.11$	$0.53 \pm 0.15 \pm 0.07$ [8]

cuts used to obtain the distributions and the corresponding total acceptances, presented in Tables 2 and 3.

To obtain the branching ratios, we divided the number of observed (corrected) events of the two modes, and divided again by the relative acceptance. The statistical error on the acceptance is negligible, and most systematic errors cancel in the relative acceptance.

For the systematic studies we varied any single cut value, as well as the parameter  $n$  for the  $\chi_F$  distribution in the Monte Carlo simulation, within some range and determined the branching ratio for every set of parameters; for the set of cuts used we did not observe evidence of any trend; all systematic variations are small compared to the statistical error and will be ignored in the final results since they would not affect the quadrature sum of the total error.

The resulting branching ratios are shown, together with previously measured values, in Table 4.

## 6. Discussion and conclusions

In Table 4 we summarize the results for the different branching ratios measured in this work. Comparing our results with previously measured ones (where available) shows good agreement.

To quantify the effects of final-state quark rearrangements in the different decays via the relevant relative matrix elements, we calculate  $\alpha$ , which is defined as the measured relative branching ratio corrected for phase space differences and, in the case of comparing CF and CS modes, for the ratio of the CKM matrix elements ( $V_{cd}/V_{cs} = 0.233 \pm 0.001$  [12]). We note that the  $\alpha$ -parameter for  $B(\Sigma^- \pi^+ \pi^+)/B(\Sigma^+ \pi^- \pi^+)$  is consistent in the decays of both the  $\Lambda_c^+$  and the  $\Xi_c^+$ . Comparing the diagrams in Figs. 1 and 2 we conclude that the source of the final-state quark does not affect the relative matrix element significantly.

In summary, we observe for the first time the Cabibbo-suppressed decay modes  $\Xi_c^+ \rightarrow \Sigma^+ \pi^- \pi^+$  and  $\Xi_c^+ \rightarrow \Sigma^- \pi^+ \pi^+$  and estimate their branching ratios. With the same analysis method we also analyze previously reported modes of both the  $\Xi_c^+$  and the  $\Lambda_c^+$  and find good agreement.

## Acknowledgements

The authors are indebted to the staff of Fermi National Accelerator Laboratory and for invaluable technical support from the staffs of collaborating institutions. This project was supported in part by Bundesministerium für Bildung, Wissenschaft, Forschung und Technologie, Consejo Nacional de Ciencia y Tecnología (CONACyT), Conselho Nacional de Desenvolvimento Científico e Tecnológico, Fondo de Apoyo a la Investigación (UASLP), Fundação de Amparo à Pesquisa do Estado de São Paulo (FAPESP), the Israel Science Foundation founded by the Israel Academy of Sciences and Humanities, Istituto Nazionale di Fisica Nucleare (INFN), the International Science Foundation (ISF), the National Science Foundation (Phy #9602178), NATO (grant CR6.941058-1360/94), the Russian Academy of Sciences, the Russian Ministry of Science and Technology, the Russian Foundation for Basic Research (grant 05-02-17869), the Secretaría de Educación Pública (Mexico) (grant number 2003-24-001-026), the Turkish Scientific and Technological Research Board (TÜBİTAK), and the US Department of Energy (DOE grant DE-FG02-91ER40664 and DOE contract number DE-AC02-76CHO3000).

## References

- [1] J.G. Körner, M. Krämer, Z. Phys. C 55 (1992) 659.
- [2] M. Bauer, B. Stech, M. Wirbel, Z. Phys. C 34 (1987) 103.
- [3] S.Y. Jun, et al., SELEX Collaboration, Phys. Rev. Lett. 84 (2000) 1857, hep-ex/9907062.
- [4] J.M. Link, et al., FOCUS Collaboration, Phys. Lett. B 512 (2001) 277, hep-ex/0102040.
- [5] J.M. Link, et al., FOCUS Collaboration, Phys. Lett. B 571 (2003) 139, hep-ex/0305038.
- [6] S. Barlag, et al., ACCMOR Collaboration, Phys. Lett. B 283 (1992) 465.
- [7] Y. Kubota, et al., CLEO Collaboration, Phys. Rev. Lett. 71 (1993) 3255.
- [8] P.L. Frabetti, et al., E687 Collaboration, Phys. Lett. B 328 (1994) 193.
- [9] J. Engelfried, et al., Nucl. Instrum. Methods A 431 (1999) 53, hep-ex/9811001.
- [10] J.S. Russ, et al., SELEX Collaboration, in: A. Astbury, et al. (Eds.), Proceedings of the 29th International Conference on High Energy Physics, World Scientific, Singapore, 1998, p. 1259, hep-ex/9812031.
- [11] F.G. Garcia, et al., SELEX Collaboration, Phys. Lett. B 528 (2002) 49, hep-ex/0109017.
- [12] W.M. Yao, et al., Particle Data Group, J. Phys. G 33 (2006) 1, cf. p. 142.